Monolithic Adsorbent-Based Rapid-Cycle Vacuum Pressure Swing Adsorption Process for Carbon Capture from Small-Scale Steam Methane Reforming

Monolithic adsorbent-based rapid-cycle vacuum pressure swing adsorption process for carbon capture from small-scale steam methane reforming

*Ishan Sharma[a], Daniel Friedrich[a], Timothy Golden[b], and Stefano Brandani[a,]**

[a] School of Engineering, The University of Edinburgh, The King's Buildings, Edinburgh EH9 3FB, UK

[b] Air Products and Chemicals, Inc., 7201 Hamilton Boulevard, Allentown, PA 18195, USA.

* Corresponding author's email address: S.Brandani@ed.ac.uk

KEYWORDS

Steam methane reforming; Small-scale; Carbon capture; Vacuum pressure swing adsorption; Monolithic adsorbent; Zeolite NaY.

ABSTRACT

Steam methane reforming is the primary route to convert natural gas into hydrogen, both at small and large-scale. Most of the effort from the scientific and industrial community has been directed towards CO_2 capture from large-scale reforming plants. This article, therefore, proposes an intensified 8-bed, 14-step vacuum pressure swing adsorption unit to capture CO_2 from a high partial pressure stream in a small-scale steam methane reforming process. The unit employs a monolithic adsorbent, rather than adsorbent pellets or beads; this allows the cycle time to be much shorter than that for pelleted adsorbent systems. The specific energy penalty for carbon capture has been minimised by regulating the blowdown and evacuation pressure, while also meeting the CO_2 purity and recovery constraints. The minimum penalty is realised when the CO_2 purity and recovery are fixed at the minimum allowable values of 95 and 90 %, respectively. The model predicts a specific electrical energy penalty of 9.03 kJ/mol CO_2 for a fixed feed processing capacity of 7.10 mol of feed/m^3/s. The corresponding productivity of the monolithic VPSA process in terms of its CO_2 production capacity was estimated to be 0.951 mol CO_2/m^3/s. The productivity was found out to be almost double than the values reported in literature for state-of-the-art MDEA based capture plants for large-scale steam methane reforming application. A dry feed gas was initially assumed for modelling; the presence of moisture was found to cause a drop in CO_2 recovery by approximately 5 percentage points. The monolithic adsorbent system has also been compared to an equally sized fixed bed, packed with pelleted adsorbent. The pelleted adsorbent system was found to have a lower working capacity between the same blowdown and evacuation pressure. The working capacity could only be improved with reducing the regeneration (evacuation) pressure, resulting in a higher vacuum pump penalty.

1. Introduction

Carbon capture from large-scale Steam Methane Reforming (SMR) has long been considered a 'low-hanging fruit' for demonstrating carbon capture[1]. The carbon dioxide (CO_2) emissions from industrial sources come in all shapes (CO_2 partial pressure) and sizes (scale). The UK government recently passed the net-zero emissions law, making it legally binding to achieve net-zero greenhouse gas emissions by 2050[2]. Carbon Capture and Storage (CCS) will be an essential part of any future portfolio of climate mitigation technologies. There have already been four demonstration plants of carbon capture from large, industrial-scale SMR[3-6]. All of these demonstration plants capture a fraction of the total CO_2 produced by the SMR process. The carbon in Natural Gas (NG) is the source of all of the direct CO_2 emissions in an SMR process. Since SMR is an endothermic process, NG is used both as the feed and fuel. The fuel NG supplies the energy needed to reform feed NG. The CO_2 from both fuel and feed NG can either be captured together or separately at different locations within the process flow scheme, leading to different scenarios for carbon capture in an SMR process. Among the different scenarios for CO_2 capture, capture from the shifted syngas stream is thermodynamically easier due to the higher partial pressure of CO_2 in this stream. Therefore, all of the four industrial demonstration plants have focused on this stream to capture CO_2. None of the demonstration plants captures CO_2 from the reformer exhaust stream, where both the mole fraction, and total pressure are significantly lower.

The Quest CCS project in Canada and the Tomakomai CCS project in Japan use an activated MDEA-based solvent for carbon capture[4,5]. Air Liquide uses the Cryocap^{TM} cryogenic process to capture ~0.1 Mt (Megatonne) per year at its Port- Jérôme site[6]. The carbon capture facility at Port Arthur, Texas (USA) uses a Vacuum Pressure Swing Adsorption (VPSA), wherein, CO_2 is

adsorbed on a Zeolite adsorbent at high partial pressure, and subsequently desorbed at vacuum. The site had captured approximately 4 Mt of CO_2 by mid-2017[7]. At the current rate, the project should have captured approximately 6 Mt of CO_2 by June 2019. Even after the end of the minimum operation period, specified as per funding requirements, the operator (Air Products and Chemicals) has still been capturing the same amount of CO_2. The CO_2 captured from the Port Arthur facility is utilised in enhanced oil recovery, thereby making a viable business case.

Small-scale modular SMR plants are kept as compact as possible and usually come only in a few standardised designs. These units are meant for small-scale customers who do not have access to an H_2 distribution network; for example, glass and steel manufacturing, metal processing, H_2 refuelling stations[8]. Collection and transportation of captured CO_2 have always been the factors which have restricted the economic viability of carbon capture in such small-scale on-site SMR units[9]. However, if there is a small-scale utilisation for CO_2, for example, when the unit is part of an industrial cluster, there can be a business case for carbon capture from small-scale SMR units[9]. Since the compactness of these small-scale SMR units is one of their key selling points, the carbon capture system has to be as compact as possible.

Rapid cycle VPSA systems, making use of structured adsorbents and/or rotary valves, are substantially smaller than the conventional VPSA systems, like the ones installed at Port Arthur. Conventional adsorption systems have adsorbent in the form of pellets or beads; they tend to suffer from a high-pressure drop at high superficial velocities. However, if the adsorbents are structured in a form like monoliths, the corresponding pressure drops are substantially lower. This, in principle, allows for shorter cycle times and thus smaller adsorbent columns. However, there is usually a trade-off between pressure drop and bulk porosity of monolithic adsorbent column, which tends to affect the heavy product's (in this case, CO_2's) purity. Structured adsorbents are

already used in industrial plants, for example, in the rapid cycle pressure swing adsorption process jointly developed by Xebec Adsorption Inc. and ExxonMobil research and engineering[10]. Structured adsorbents also have a long track record of being utilised in a variety of different applications, like air dehumidification, vehicle exhaust treatment, etc. There has also been an interest in employing structured adsorbents in carbon capture applications. For example, Mohammadi[11] tested a corrugated monolith for carbon capture from the flue gas of a coal-fired power plant. Rezaei *et al.*[12] also investigated employing a monolithic adsorbent for post-combustion carbon capture. Rotary valves can decrease the valve response time and system's dead volume. Due to a reduction in the extent of piping and the number of valves required, they often represent a cost-effective option to the conventional solenoid valves.

Recently, another complementary approach to achieve intensification of the SMR process with carbon capture has been reported[13]. The approach focusses on combining the CO_2 VPSA and the H_2 PSA into a single separation unit, capable of producing both CO_2 and H_2 at purities and recoveries greater than 95 and 90 %, respectively. Streb *et al.*[13] report productivities in the range of 1.01-to-1.52 mol $CO_2/m^3/s$, which is significantly greater than those reported in the open literature for absorption-based CO_2 capture from H_2 production plants[13]. The corresponding electrical energy consumed ranged from about 22.0-to-48.4 kJ/mol CO_2[13].

Membrane-assisted[14] and chemical looping reforming[15], along with their combination, are some of the alternative technologies that have been suggested in the literature for carbon capture from the SMR process. Recently, there have also been attempts at combining membrane and Pressure Swing Adsorption (PSA) technologies for simultaneous production of H_2 and CO_2 from a small-scale SMR process[16]. If a commercial adsorbent is used in the VPSA process, the technology

readiness level of this technology is expected to be higher than emerging technologies like Membrane-assisted reforming and/or chemical looping.

The present work was carried out as part of a wider project looking into developing designs of modular, compact, rapid-cycle adsorption units for CO_2 capture from a variety of small-to-medium-scale industrial sources. Carbon capture from small-scale SMR represents a case study which covers a broad spectrum of the CO_2 partial pressures observed in industrial emission streams. The use of structured adsorbents for carbon capture from SMR process has not been explored in the scientific literature, even while, based on the arguments above, it appears to be one of the promising solutions to achieve intensification of the process; this becomes critically important for small-scale SMR processes. This paper aims to bridge this knowledge gap by designing a rapid-cycle VPSA process utilising a monolithic adsorbent. In line with the experience with large-scale SMR, this study also focusses on capturing the CO_2 from the high partial pressure stream, i.e., the easy-to-capture fraction of the CO_2. The carbon capture from small-scale SMR appears relevant, especially considering the fact that the scale of CO_2 utilisation is typically small as well[17]. In principle, the same technology should also be applicable to carbon capture from a large-scale SMR process.

2. Small-scale SMR process in brief

Both small and large-scale SMR processes primarily use the same underlying technology. A small-scale SMR process differs from a large-scale SMR process with regards to the operating conditions and the overall system configuration. For example, the reforming conditions are less severe in small-scale SMR. A small-scale SMR unit has fewer unit operations to keep the system compact. A small-scale SMR unit also differs from a large-scale SMR plant in terms of overall

system configuration. Small-scale SMR units come as a 'plug-and-play' device and are not usually integrated with any other process plant on-site, which is not the case with large-scale SMR plants which are highly integrated both within themselves, as well as with other process plants in the vicinity. For a detailed explanation of the SMR process, in particular, small-scale SMR, the reader is referred to our prior work[18]. The details about the mass and energy balance (in UniSim®) are also given in Sharma *et al.*[18].

NG (primarily methane) is the typical feedstock of the SMR process. The primary SMR reaction is given as reaction (1) below:

$$CH_4(g) + H_2O(g) + Heat \leftrightarrow CO(g) + 3H_2(g) \quad (1)$$

CH_4: Methane

H_2O: Water/Steam

CO: Carbon monoxide

A separate stream of fuel NG is burned to provide the energy needed to perform the reforming reaction (1). The CO_2 thus formed is diluted in N_2 and can be captured from Location III in Figure 1. Due to the low partial pressure of CO_2 in this stream, carbon capture from this stream is thermodynamically energy-intensive. The other source of carbon in an SMR plant is the CO_2 produced due to the carbon present in the feed NG. The Shift reactor is the next processing step after reforming. The water-gas shift reaction (reaction, 2) involves the reaction of CO and the surplus steam fed during the reforming step, in the presence of a suitable catalyst[19].

$$CO(g) + H_2O(g) \leftrightarrow CO_2(g) + H_2(g) + Heat \quad (2)$$

Water-gas shift reaction is followed by condensing out as much excess water as possible with the help of cooling water. At this stage, the maximum possible conversion of carbon to CO_2 has been achieved. After condensate removal, the shifted syngas (primarily, H_2 and CO_2) is fed to the

H_2 PSA. The H_2 PSA produces the high purity H_2 product, as per the downstream process requirement. The waste stream produced by the H_2 PSA has a significant calorific value and is thus mixed with fuel NG to be burned in the reformer.

The CO_2 from the process stream can be captured either at location I, location II, or along with the CO_2 from fuel stream at location III (Figure 1). Due to the thermodynamic arguments presented before, it makes economic sense to capture the maximum amount of CO_2 at high partial pressure. In a typical small-scale SMR process, CO_2 partial pressures at locations I and II are 1.7 bar, and 0.5 bar, respectively[18]. If all of the CO_2 is captured at location III, the maximum possible partial pressure at that location is 0.2 bar. The higher partial pressure of CO_2 at location I makes it conducive for CO_2 capture. Due to the relatively higher partial pressure of CO_2 at location I, VPSA appears to be a promising technology for carbon capture. For carbon capture from reformer flue gas, a technology like Temperature Swing Adsorption (TSA) might be an alternative to the VPSA which requires very low regeneration pressures to maximise the working capacity. Inventys Inc., a Canadian firm, has recently patented a process named VeloxoTherm™ (velox: fast; therm: thermal) for post-combustion CO_2 capture *via* a rapid TSA cycle and structured adsorbents[20]. A monolithic adsorbent-based TSA process deserves significant attention due to the low partial pressure of CO_2 in the stream, along with the presence of moisture. Developing such a system for the reformer flue gas is beyond the scope of the present study.

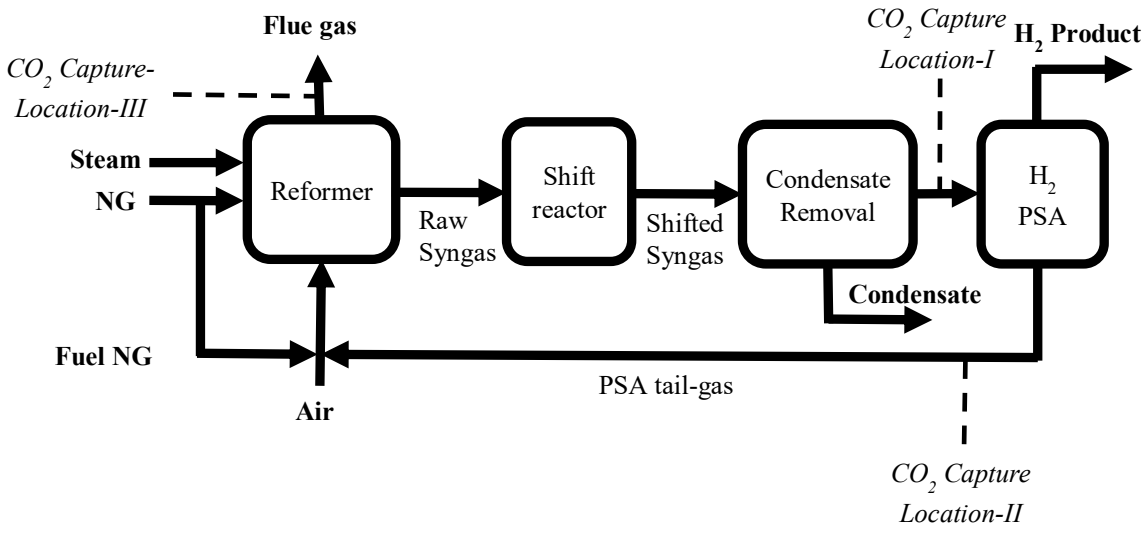

Figure 1. Typical processing steps in SMR

3. Adsorbent and the VPSA process

Zeolite 13X is the benchmark adsorbent for VPSA-based carbon capture from flue gas streams at near atmospheric pressure[21]. This is mainly due to the high working capacity and selectivity of 13X for CO_2. However, due to its high Henry's law constant, the CO_2 isotherm is almost rectangular (Figure 2). This implies that in order to realize the high working capacity, the regeneration pressures have to be extremely low. The CO_2 isotherm on Zeolite NaY is, however, a bit less steep, as shown for a typical NaY and 13X sample at 303.15 K.

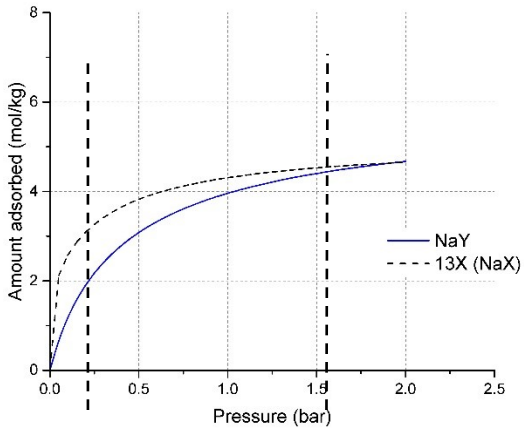

Figure 2. Representative CO_2 isotherms at 303.15 K on NaY[22] and 13X (NaX)[23].

The partial pressure of CO_2 in the shifted syngas stream, after condensate removal, is higher than that in typical coal-based flue gas (~1.7 bar vs. 0.15 bar). NaX is the adsorbent of choice for carbon capture from flue gas mainly due to the shape of the isotherm, which ensures a significant uptake of CO_2 at such low partial pressures. For the present application, NaY has been chosen as the adsorbent because of its higher working capacity between the feed pressure and a relatively moderate desorption (or evacuation) pressure. Rastelli *et al.*[24] also noted that NaY-based zeolites performed better than 13X-based adsorbents in terms of higher CO_2 working capacity in a similar application. NaY has also been investigated for other carbon capture applications[25, 26].

The typical feed gas properties have been summarised in Table 1. The feed contains about 0.45 % moisture. Among all of the components present in the feed, water has the highest Henry's law constant, indicating the strongest attraction, followed by CO_2; all the water present in the feed is therefore expected to go with the CO_2 product. Also, the CO_2 product needs to be dehydrated before being fed for sequestration. The 'effective' CO_2 purity is therefore not affected by water presence. The amount of moisture in the feed is also rather low as compared to typical flue gas streams. Therefore, in order to optimise the computational effort, the feed to the VPSA has been assumed to be completely dry in the first instance, followed by an estimation of the relative effect

of moisture presence in the feed. Table S1 (supporting information) lists the attributes of the NaY monolith column assumed in this study. Figure 3 shows an individual channel of the square monolith.

Table 1. Feed gas properties at location I.

Feed flow rate	14.3529 mol/s
Feed temperature	303.15 K
Feed Pressure	9.88 bar
Composition (mol %)	
CH_4	2.66
N_2	0.12
CO_2	17.24
H_2	76.69
CO	2.84
H_2O	0.45

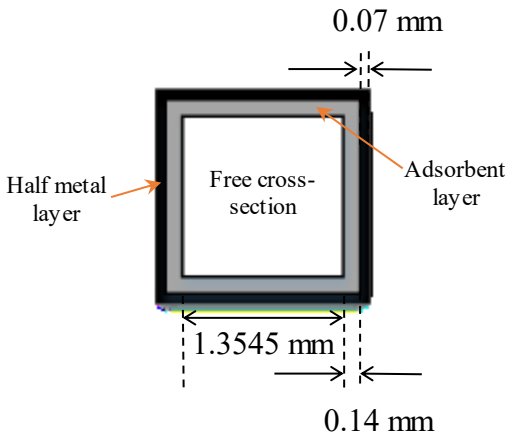

Figure 3. An individual square channel in the NaY monolith

The isotherm data for different constituent species on NaY has been taken from the literature as follows:

CO_2 and N_2- Shao *et al.*[22], CH_4- Talu *et al.*[27], CO- Walton and LeVan[28], H_2- Raj *et al.*[29] and H_2O- Piers *et al.*[30]

The data have been fitted to pure dual-site Langmuir isotherms and extended to predict multi-component equilibria. The isotherm data and fits have been shown in Figure S1 (supporting information).

Figure 4 shows the 8-bed, 14-step VPSA cycle, and its schedule. The cycle is based on one of the configurations reported in Hsu *et al.*[31] for an 8-bed VPSA system for CO_2 capture from shifted syngas.

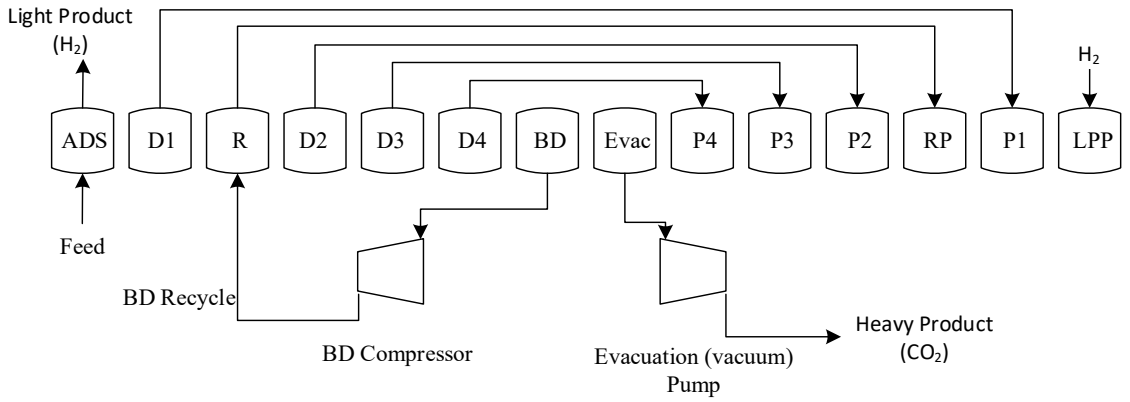

(a)

Bed-1	ADS		D1	R	D2	D3	D4	BD	Evac		P4	P3	P2	RP	P1	LPP
Bed-2	D1	R	D2	D3	D4	BD	Evac		P4	P3	P2	RP	P1	LPP	ADS	
Bed-3	D2	D3	D4	BD	Evac		P4	P3	P2	RP	P1	LPP	ADS		D1	R
Bed-4	D4	BD	Evac		P4	P3	P2	RP	P1	LPP	ADS		D1	R	D2	D3
Bed-5	Evac		P4	P3	P2	RP	P1	LPP	ADS		D1	R	D2	D3	D4	BD
Bed-6	P4	P3	P2	RP	P1	LPP	ADS		D1	R	D2	D3	D4	BD	Evac	
Bed-7	P2	RP	P1	LPP	ADS		D1	R	D2	D3	D4	BD	Evac		P4	P3
Bed-8	P1	LPP	ADS		D1	R	D2	D3	D4	BD	Evac		P4	P3	P2	RP

(b)

Figure 4. The 8-bed, 14-step VPSA cycle (a), and its schedule (b). ADS: Adsorption, D1: First de-pressurisation (equalisation), R: Rinse step, D2: Second de-pressurisation (equalisation), D3: Third de-pressurisation (equalisation), D4: Fourth de-pressurisation (equalisation), BD: Blowdown, Evac: Evacuation, P4: Fourth pressurisation (equalisation), P3: Third pressurisation (equalisation), P2: Second pressurisation (equalisation), RP: Rinse pressurisation, P1: First pressurisation (equalisation), and LPP: Light product (H_2) pressurisation

The cycle starts with one of the beds (bed-1) receiving the feed mixture, and producing a light product almost devoid of any CO_2. This is followed by the first de-pressurisation (equalisation) step, where the light product end exhaust is used to pressurise another bed (bed-7). The rinse step involves the heavy product end of the bed receiving the BD recycle stream from bed-3, undergoing BD step. During the rinse step, another stream is taken from the light product end of the bed and

is used to pressurise bed-6, undergoing rinse pressurisation step. The BD recycle stream is mainly composed of the heavy product (ideally, >90 % by mol). The heavy product end is enriched by the BD recycle. The rinse step is followed by three de-pressurisation (equalisation) steps, which are followed by the BD step. Next, the bed is evacuated to vacuum pressure to generate the heavy product. The bed further undergoes three consecutive pressurisation (equalisation) steps from the light product end. This is followed by the rinse pressurisation, another pressurisation, and the LPP step. A part of the final H_2 product (>99.999 % by mol) is used to pressurise the bed up to near feed pressure during the LPP step. The effective working capacity of the bed is between the CO_2 partial pressure at the end of the BD step and evacuation pressure. In the sequence of steps, the rinse step is executed only after the first pressure equalisation step to avoid having to pressurise the BD recycle stream to the feed pressure. The different pressure equalisations, rinse/RP, LPP, and BD steps have been assumed to be of the same duration; this is based on a patent[31] for CO_2 capture from a similar stream. Similarly, the duration of adsorption and evacuation steps has been taken to be double that for the other steps. The cycle time of a typical H_2 PSA employing pelleted adsorbents is ~800s[32]. For the monolithic adsorbent VPSA, a quarter of that, i.e. 200 s, has been taken as the cycle time; this represents a potential four-fold decrease in column volume.

4. The VPSA process model

The authors have used their in-house cyclic adsorption process simulator, CySim, to model the VPSA process cycle[33]. The monolith column module has been added to the pool of modules available in CySim. CySim uses the finite volume method with a flux limiting scheme. CySim uses the state-of-the-art differential-algebraic equation solver SUNDIALS. The CySim simulation

models only one of the beds, as per the unibed approach[34]. The monolith column module code has been validated against the experimental breakthrough results reported in Ahn and Brandani[35].

Following is a summary of the CySim model assumptions:

- Ideal gas behaviour
- Fully developed laminar flow in individual channels. The calculated Reynolds number at feed inlet conditions is 82.42.
- 1-D axially dispersed plug flow in bulk fluid phase
- The moisture content in the feed gas is assumed to go with the heavy product
- Isothermal operation: It has been assumed that due to the high thermal mass and conductivity of the metal base-layer, the heat generated during adsorption is quickly absorbed and dissipated throughout the metal matrix, keeping the system nearly isothermal. With 13X, Mohammadi[11] observed isothermal operation for an equal thickness of the adsorbent and metallic layer when experimenting with VPSA-based CO_2 capture from flue gas (from coal-firing). With NaY, in the present application, the amounts adsorbed are expected to be higher, given the higher partial pressure of CO_2 in the feed. Nevertheless, the heat of adsorption for NaY is lower than that for 13X. The overall effect of these two contributions is challenging to estimate *a priori*. In any case, the system could be made to behave isothermally by varying the relative thickness of the metal layer *vis-à-vis* that of the adsorption layer.
- 1-D diffusion in the adsorbent layer with mass transfer rate given by the LDF model. Ahn and Brandani[36] demonstrated that the 3-D mass diffusion in the adsorbent layer could in-effect be modelled as a 1-D phenomenon if the adsorbent layer thickness is corrected to take into account the extra path a molecule has to diffuse through at the four

corners of a monolith made up of rectangular channels. The diffusivity of the constituent species in the adsorbent layer (D_s) is assumed to be given by Eq. (3). The molecular diffusivities at feed Temperature have been taken from Luberti *et al.*[37].

$$D_s = \frac{\varepsilon_{ad}}{\tau_{ad}} D_m \tag{3}$$

- Mass transfer in the micropores has been assumed to be fast, with the entire adsorbent crystal being at equilibrium with the fluid at the surface.
- The pressure gradient in the axial direction is given by Eq. (4)[38]:

$$\frac{dP}{dz} = 28.47 \frac{v\,\eta}{h^2} \tag{4}$$

The model equations are as follows:

For j = 1, 2…NC

Component mass balance:

$$\frac{\partial c_j}{\partial t} + \frac{(1-\varepsilon_{bulk})}{\varepsilon_{bulk}} \frac{\partial \overline{Q_J}}{\partial t} + \frac{\partial (v.c_j)}{\partial z} + \frac{\partial J_j}{\partial z} = 0 \tag{5}$$

$$\varepsilon_{ad} \frac{\partial c_{ad,j}}{\partial t} + (1-\varepsilon_{ad}) \frac{\partial \overline{q_J}}{\partial t} = \frac{\partial \overline{Q_J}}{\partial t} \tag{6}$$

$$\frac{\partial \overline{Q_J}}{\partial t} = k_{LDF,j}(c_j - c_{ad,j}) \tag{7}$$

$$k_{LDF,j} = \frac{3D_{s,j}}{w_c^2}$$

$$w_c = w\left(1 + \frac{w}{h}\right)$$

$$\overline{q_J} = q_j^*(c_{ad,j}) \tag{8}$$

$$\frac{\partial J_j}{\partial z} = -D_{m,j} c_T \frac{\partial y_j}{\partial z} \tag{9}$$

Boundary conditions:

$$J_j\big|_{z=0} = \left(\frac{v+|v|}{2}\right)\Big|_{z=0} \left(y_{j,0-} - y_j(0)\right) c_T$$

$$J_j\big|_{z=L} = \left(\frac{v+|v|}{2}\right)\Big|_{z=L} \left(y_{j,L+} - y_j(L)\right) c_T \tag{10}$$

Dual-site Langmuir isotherm:

$$q_j^* = \frac{q_{j,s}^1 b_j^1 p_j}{1+\sum_{k=1}^{NC} b_k^1 p_k} + \frac{q_{i,s}^2 b_i^2 p_i}{1+\sum_{k=1}^{NC} b_k^2 p_k};$$

$$b_j^l = b_{j,0}^l exp\left(\frac{\Delta \tilde{H}_j^l}{RT}\right) \quad (11)$$

The extended dual-site Langmuir isotherm has been used to predict the multi-component isotherms. The procedure detailed in Farmahini *et al.*[39] has been used to fit the isotherm parameters. The pure component isotherm data for CO_2 was fitted first at the lowest temperature i.e., 303.15 K, to obtain the saturation capacity for both the sites. Assuming that every component has access to each of the adsorbent sites, the saturation capacity ($q_{j,s}^1$, and $q_{j,s}^2$) of both the sites is taken to be the same for all the species (except water, which has a much higher saturation capacity). Furthermore, since the isotherms for N_2 and CO are straight lines, the affinity parameters ($b_{j,0}^1$, and $b_{j,0}^2$) for both the sites have been taken to be the same. The fitted dual-site Langmuir isotherms are listed in Table S2 (supporting information).

5. Results and discussion

After fixing the monolith geometry and step times, as explained above, and assuming complete pressure equalisation during the different equalisation and rinse/RP steps, there remain two degrees of freedom which could be used to fine-tune the unit's performance to achieve 95 % purity and 90 % recovery of CO_2. The two degrees of freedom are the BD and evacuation pressure (P_{Evac}), respectively. In the CySim model, the BD pressure is regulated by the flow through the BD compressor, which is given by Eq. (12) as follows:

$$F_{BD} = F_{max} - \chi(\Delta P)^2 \quad (12)$$

A 3×3 factorial design has been considered here to analyse the effect of F_{max} and P_{Evac} on CO_2 purity, recovery, specific energy penalty and productivity of the VPSA system. The productivity of the unit can either be calculated on the system's ability to process feed (Eq. 13) or to produce CO_2 product (Eq.14). Since κ_{Feed} is based on feed flow rate, it would stay fixed, once the cycle time and the volume have been fixed.

$$\kappa_{Feed} = \frac{m_{Feed}}{(CT)(V_{bed})} \quad (13)$$

$$\kappa_{CO_2} = \frac{m_{CO_2}}{(CT)(V_{bed})} \quad (14)$$

The specific energy (electricity) penalty ($\dot{E}_{CO_2}$) has been estimated using Eq. (15) as follows:

$$\dot{E}_{CO_2} = \frac{E_{BD}+E_{Evac}}{m_{CO_2}} \quad (15)$$

Table 2 reports the performance parameters listed above for different combinations of F_{max} and P_{Evac} within the range of 6.8-to-7.4 and 0.25-to-0.4, respectively. The ranges were determined by a trial and error procedure. All the operating points have the same feed processing ability (κ_{Feed}) of 7.10 mol of feed/m^3/s. The overall efficiencies of the BD compressor and the vacuum pump have been assumed to be 0.7 and 0.5, respectively. The CySim simulation only pressurises the CO_2

product up to atmospheric pressure; pressurisation of CO_2 to supercritical state has not been included here.

Table 2. The 3×3 factorial design for F_{max} and P_{Evac}. P_{CO_2}- Purity of CO_2 product stream (%), and R_{CO_2}- Overall recovery of CO_2 in CO_2 product stream (%).

	$P_{Evac} = 0.25$ bar			$P_{Evac} = 0.325$ bar			$P_{Evac} = 0.4$ bar		
	P_{CO_2} (%)	R_{CO_2} (%)	$\dot{E}_{CO_2}$ (kJ/mol CO_2)	P_{CO_2} (%)	R_{CO_2} (%)	$\dot{E}_{CO_2}$ (kJ/mol CO_2)	P_{CO_2} (%)	R_{CO_2} (%)	$\dot{E}_{CO_2}$ (kJ/mol CO_2)
$F_{max} = 7.4$ mol/s	95.12	94.29	11.61	96.88	89.52	9.98	98.11	82.98	9.02
$F_{max} = 7.2$ mol/s	94.47	94.57	11.40	96.13	90.12	9.75	97.33	83.50	8.58
$F_{max} = 6.8$ mol/s	93.58	94.71	11.04	95.01	90.68	9.34	96.08	84.07	8.15

From the solutions reported in Table 2, a general trend is evident that $\dot{E}_{CO_2}$ tends to decrease with decreasing F_{max} and increasing P_{evac}. Typically, $\dot{E}_{CO_2}$ also tends to decrease with decreasing quality (purity) and quantity (recovery) of the CO_2 product. The minimum specific energy penalty is expected to be at the minimum allowable CO_2 purity and recovery of 95 % and 90 %, respectively. Starting from the solution at $F_{max} = 6.8$ mol/s and $P_{evac} = 0.325$ bar, another operating point can be obtained by slightly decreasing F_{max} and increasing P_{evac}, simultaneously. At $F_{max} = 6.72$ mol/s and $P_{evac} = 0.337$ bar, the CO_2 product's purity and recovery are 94.94, and 89.96 %, respectively; the corresponding $\dot{E}_{CO_2}$ for this point is 9.03 kJ/mol CO_2 (electrical). Figures 5 shows the pressure profile of the bed during the 14-step cycle, respectively. The strange

trajectory of the column pressure during the rinse step is due to the manner in which the inflow and outflow to the column have been defined in this work; both of them have been expressed as a *different* function of the pressure difference during the rinse and rinse pressurisation step. While the incoming flow is given by Eq. (11), the outgoing flow is proportional to the square root of the pressure difference. As a result, at the start of the rinse step, there is a net outflow from the monolith column which decreases the column pressure to a minimum, after which it starts to receive a net inflow due to the now decreased pressure difference.

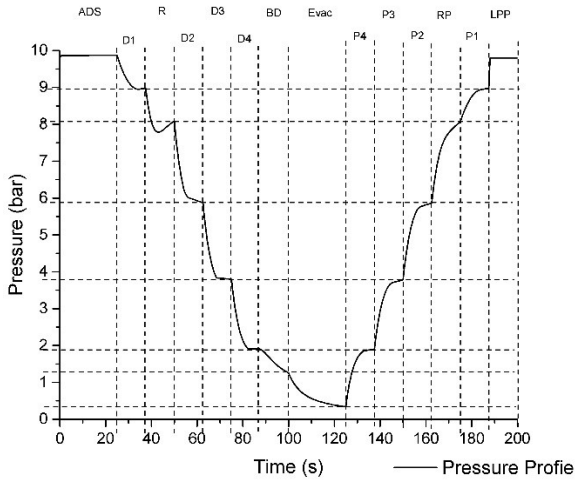

Figure 5. The pressure profile of the bed, during the VPSA cycle, as predicted at the heavy product end.

The energy for carbon capture is provided in the form of electricity to the BD compressor and evacuation pump. The evacuation pump accounts for 70% of the energy input, while the BD compressor accounts for the rest. Furthermore, compressor and pump inefficiencies account for ~40 % of the total electrical energy penalty. Efficiency improvements could result in significant savings in terms of energy penalty. Since the capture unit requires energy in the form of electricity, renewable electricity could directly be utilised, if available; this should limit the CO_2 emissions associated with electricity production.

The light product (H_2) produced from the CO_2 VPSA unit still has 8.74 % impurities. In a Greenfield design of the small-scale SMR unit, the CO_2 VPSA can drastically reduce the load on the H_2 PSA. As a result, a significantly smaller H_2 PSA can be designed to meet the purity specifications. Ideally, the H_2 PSA could also employ monolithic adsorbents to intensify the process further. In a Brownfield design, the CO_2 VPSA can be placed in between the condensate removal step and H_2 PSA. In this case, the original H_2 PSA can still be used for H_2 purification, as is done at a large-scale SMR facility at Port Arthur.

Penalty due to the presence of water vapour in feed-

Water is more strongly attracted by the NaY adsorbent, compared to CO_2. Since the 14-step cycle includes the counter-current evacuation step, the water adsorption front is expected to stay confined towards the feed end. In order to estimate the impact of water vapour presence, the CySim model is re-evaluated for a moist feed (Table 1). The water isotherm at 303 K has been sourced from Piers *et al.*[30]. The isotherm has been shown in Figure S1 (f) (supplementary information). The Henry's law constant (the product of saturation capacity and Langmuir affinity parameter) for water isotherm is about 572 times that of CO_2. The BD and evacuation pressure levels have been kept at 1.250 and 0.337 bar, respectively, the same as for dry feed conditions. Figure 6 (a) shows the approach to cyclic steady state in terms of recovery and purity (on a dry basis). These vary rapidly over the initial 200 cycles and then change very slowly approaching approximately 85% and 97%, respectively. The improvement on the purity is a result of the fact that under moist conditions the main impurity of the CO_2 rich stream is water, which can be condensed and removed before compression. The slight fall in CO_2 recovery is primarily due to the substitution of CO_2 by H_2O in the adsorbed phase. To counter the loss of CO_2 from the light product's end, during the

adsorption step, the adsorption time can be slightly reduced, while sacrificing a bit in terms of the effective CO_2 purity. Figure 6 (b) shows the adsorbed phase concentration of CO_2 and H_2O for moist feed conditions after over 1300 cycles; for comparison, the CO_2 adsorbed phase profile for dry feed conditions has also been shown. The adsorbed water front is restricted to the initialportion of the column's length due to the high Henry's law constant and low amounts of water vapour present in the feed.

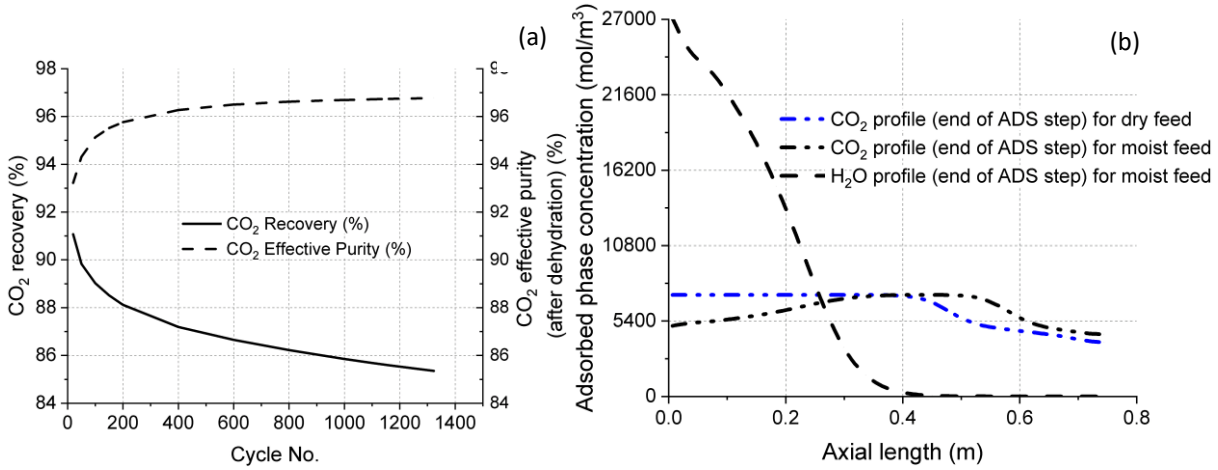

Figure 6. (a) Approach to CSS for moist feed conditions; (b) CO_2 and H_2O adsorbed phase concentration at the end of the adsorption step for moist and dry feed conditions.

Temperature swing management-

The mass balance of CO_2 and H_2O at cyclic steady state provides the moles of CO_2 and H_2O getting adsorbed during the adsorption step. Fast heat dissipation across the adsorbent and metallic layer can be assumed because of the small thickness (of the adsorbent layer) and high thermal conductivity (of the metallic layer). Assuming a constant heat of adsorption of about 30 and 75 kJ/mol for CO_2 and water, respectively, a temperature swing of approximately 13 °C is estimated during the adsorption step. The temperature swing can however be curtailed by increasing the thermal mass of the metallic layer. For example, doubling the metallic thickness leads to a

temperature swing of approximately 7.5°C. However, the increased metallic layer thickness also leads to a fall in the productivity of the system by about 14 % (0.951 from 1.107 mol $CO_2/m^3/s$).

Pelleted vs. monolithic- column

The performance of the monolithic column is assessed in comparison to an equally sized pelleted column. The radius of such a pelleted column, occupying the same volume as that of the structured-column, comes out to be 0.353 m; this is assuming a metal layer half-thickness of 14 mm (i.e. double of that in Figure 3). Other characteristics of the adsorbent and the packed bed have been summarised in Table S3 (supplementary material). Unlike the structured-adsorbent, the pelleted adsorbent column has been modelled under the non-isothermal assumption, due to the absence of a heat 'sink', like the metallic layer. Another fundamental difference between the two cases is that the characteristic diffusional length in case of monolithic adsorbent (i.e., the adsorbent layer thickness) is about an order of magnitude smaller than in the case of pelleted adsorbent (i.e., the pellet radius); this implies that for the same pore diffusivity, the LDF mass transfer co-efficient for structured-adsorbent should be a hundred times larger than that for pelleted adsorbent. The rate of mass transfer from the gas-phase to adsorbed-phase has been assumed to be macropore diffusion controlled, with the pore diffusivity estimated from molecular diffusivities at feed temperature[37]. The fixed bed has been assumed to follow the same sequence and duration of steps as in the case of monolithic column. The BD and evacuation pressure levels have been kept the same as that for the monolithic solution. The CO_2 purity and recovery thus obtained are 83.63 and 84.62 %, respectively. It is important to note here that due to the difference in bulk porosities, the pelleted column would have more adsorbent than monolithic column; this is because both of them have the

same volume. The fall in purity is primarily an indication of the pelleted column being underutilised, as evident from the CO_2 adsorbed phase concentration profile in Figure 7.

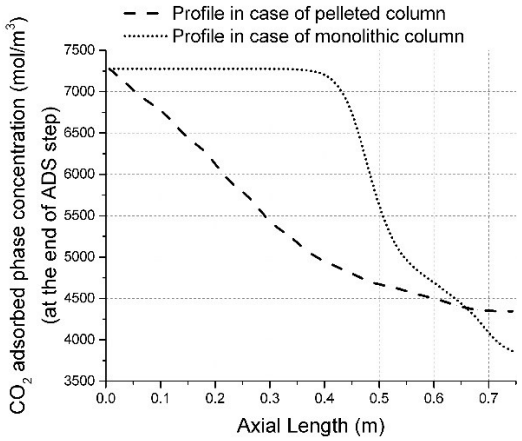

Figure 7. CO_2 adsorbed phase concentration profile in the axial direction.

The temperature swings observed in the case of the pelleted column are significantly higher, as shown in Figure 8. The low thermal conductivity of zeolite, in comparison to metal, is the primary reason for such higher, localised swings.

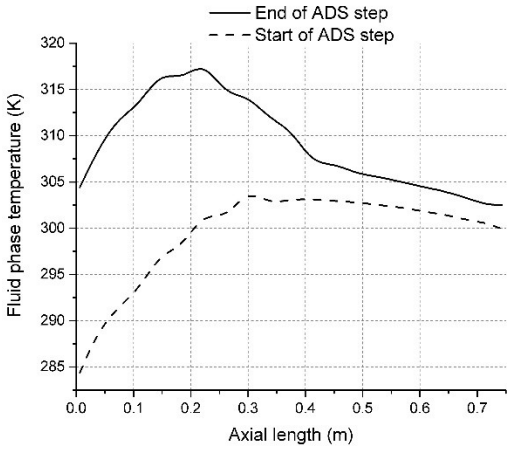

Figure 8. Temperature profile in the axial direction for pelleted column.

The CO_2 purity can be improved by increasing the cycle time, thereby also leading to a further reduction in CO_2 recovery. Table 3 shows a sensitivity analysis with respect to the cycle time.

Table 3. Sensitivity analysis with respect to the cycle time (pelleted column).

P_{BD} =1.25 bar P_{Evac} =0.337 bar	P_{CO_2}(%)	R_{CO_2}(%)
$CT = 240$	86.77	81.97
$CT = 300$	95.99	79.99
$CT = 400$	99.84	70.25

The CO_2 recovery can simultaneously be increased only with a decrease in evacuation pressure (P_{Evac}). Therefore, to achieve the same CO_2 product purity and recovery in the pelleted column, the evacuation pressure has to be lower, as compared to the monolithic column. A lower evacuation pressure implies a higher specific energy penalty for the vacuum pump. Since the total volume of the pelleted and the monolithic column is the same, a CO_2 recovery of 95 % in both the cases, implies the same productivity as well (irrespective of the cycle times). Therefore, for the same purity, recovery and productivity of the two cases, the monolithic column should exhibit a lower specific energy penalty for the vacuum pump, as compared to the pelleted column. It is important to note here that as per the preceding discussion, the vacuum pump is responsible for the majority (70 %) of the energy penalty.

Comparison with literature values-

Out of the four industrial CO_2 capture demonstration projects in large-scale SMR plants, two use a variant of MDEA solvent[18]. Information is available in open literature for one of them, i.e. the Quest carbon capture and storage project[40]. A recent IEAGHG study has also looked into the design of an MDEA-based CO_2 capture unit for large-scale SMR process[41]. To ensure that the comparison between different forms of energies is meaningful, the thermal energy (reboiler duty)

is converted to exergy with the help of Carnot factor[13]. The total exergy input to the MDEA process is thus given by Eq. 16. In contrast, the exergy input to the VPSA process is only in the form of shaft work.

$$\dot{E}x_{MDEA} = \left(Q_{Reb} \left(1 - \frac{T_{amb}}{T_{Reb}} \right) \right) / \dot{m}_{CO_2} + \dot{E}x_{Shaft\ Work} \quad (16)$$

Table 4 shows examples of the specific exergy input and productivity values from literature for MDEA-based capture in SMR processes. The system volume used for productivity calculations is the total volume of absorber(s) and stripper.

Table 4. Specific exergy input and productivity of MDEA process from literature.

	Specific exergy input, $\dot{E}x_{MDEA}$ (T_{amb} =303 K)	Productivity, κ_{CO_2}	Remarks
Quest carbon capture project[40] (CO_2 partial pressure in feed = 5.05 bar)	26.55 kJ/mol CO_2	0.425 mol CO_2/m^3/s	Q_{Reb} ~ 82 MW (thermal) T_{Reb} = 414.15 K $\dot{m}_{CO_2}$ ~ 1 Mt/y Total absorber (three in number) and stripper column volume- 1695.80 m^3 R_{CO_2} = 82 % (@ ~ 1.5 bar) P_{CO_2} = 99.27 %
IEAGHG Technical Report[41] (CO_2 partial pressure in feed = 4.23 bar)	18.25 kJ/mol CO_2	0.531 mol CO_2/m^3/s	Electricity generation penalty due to CO_2 capture ~ 5.369 MW (electrical) $\dot{m}_{CO_2}$ ~ 0.40 Mt/y Total absorber and stripper column volume- 553.51 m^3 R_{CO_2} = 98.61 % (@ ~ 2.9 bar) P_{CO_2} = 99.94 %

The monolithic VPSA process's productivity is approximately twice as that for MDEA solvent-based capture processes. The specific exergy input (9.03 kJ/mol CO_2) to the VPSA process is also predicted to be lower than those for MDEA-based capture.

As mentioned in the introduction, Streb *et al.*[13] have also recently looked at intensification of carbon capture in SMR process by combining the H_2 PSA and CO_2 VPSA in a single unit. Streb *et al.*[13] looked at the trade-offs between the specific exergy input and productivity for this single VPSA unit under the following set of constraints- R_{CO_2}, $R_{H_2} \geq 90$ % and P_{CO_2}, $P_{H_2} \geq 95$ %. In comparison, the operating point reported in this article corresponds to hydrogen recovery and purity of 99.7 % and 91.26 %, respectively. Another significant difference between Streb *et al.*[13] and the present analysis is the difference in feed pressure. The CO_2 partial pressure in the present case is 4.4 times smaller than that in Streb *et al.*[13] (1.70 bar vs. 7.5 bar). Figure 9 compares the performance reported by Streb *et al.*[13] and the present study.

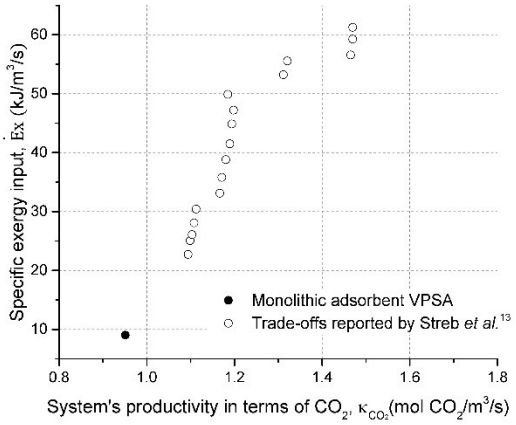

Figure 9. A comparison of monolithic adsorbent VPSA designed in this work and the exergy-productivity trade-offs reported by Streb *et al.*[13].

The specific exergy input for the structured VPSA design is lower than the range reported in Streb *et al.*[13]. It is important to note here that the working capacity of the adsorbent (activated carbon) chosen by Streb *et al.*[13] is typically lower than NaY. Therefore, the evacuation pressure needed to achieve the same CO_2 working capacity is also typically lower for activated carbon, as compared to NaY. Indeed, the evacuation pressures reported by Streb *et al.*[13] (<0.1 bar) are lower

than those reported in this work (0.337 bar). The lower evacuation pressure might be the primary reason for the higher energy consumption reported in Streb *et al.*[13]. Nevertheless, the idea of using a single separation unit, instead of two, appears to be a promising approach to further intensify the SMR process, with carbon capture. Even though the fluid interstitial velocity, during the adsorption step, for the monolithic column is higher than that reported by Streb *et al.*[13] (0.18 vs. 0.10 m/s, respectively), the productivity of the monolithic VPSA process is lower than the range reported by Streb *et al.*[13]. One of the reasons for this might be the different systems pressures; the feed pressure in Streb *et al.*[13] is approximately three time greater. Nevertheless, the productivity of the monolithic VPSA process can be further increased by decreasing the cycle time and the number of channels, while also increasing the thickness of the adsorbent layer. As the adsorbent layer thickness increases, the mass transfer co-efficient decreases; at one point it should start to significantly degrade process performance. To identify this tipping point is outside the scope of the present study. However, the encouraging performance predicted by these simulations does indicate that monolithic adsorbents might be a worthwhile option to investigate for carbon capture applications, particularly where intensification of such processes is a requirement.

6. Conclusions

This study has presented a design for a modular CO_2 capture process capable of separating up to 60% of the emissions from a small-scale SMR process, which can be captured efficiently due to the higher partial pressure of CO_2 in the shifted syngas stream. The use of NaY zeolite allows to run the process with high productivity and reasonable requirements on the vacuum system (approximately 0.33 bar). The design includes the use of a monolithic adsorbent, which is critical here as it allows the cyclic adsorption-based separation processes to operate at shorter cycle times

and faster interstitial velocity, thereby reducing the amount of adsorbent required, and thus the system volume as well. The cycle time for the monolithic column-equipped VPSA process is 200 s, representing a four-fold drop from the cycle time of a typical H_2 PSA. An 8-bed, 14-step VPSA cycle has been modelled in our in-house adsorption process simulator, CySim. The system is modelled initially assuming a dry feed; the effect of moisture presence in the feed has been quantified later. Two degrees of freedom have been identified in the design exercise: the evacuation and blowdown pressures. A 3×3 factorial design has been used to analyse the individual, and the combined effect of these two parameters on CO_2 purity, recovery, and specific energy penalty. Based on the trends observed, an operating point has been chosen which satisfies the purity and recovery constraints, while also minimising the specific energy penalty. This operating point corresponds to an energy (electricity) penalty of 9.03 kJ/mol. The moisture presence in the feed, using the same conditions for the dry feed, has been found to decrease the CO_2 recovery by approximately 5 % while the purity on a dry basis increases by 2 %. This indicates that the process can be run under moist conditions and achieve both high purity and recovery. . An equally-sized packed bed, filled with the pelleted adsorbent, has also been modelled and found to be unable to achieve the minimum recovery requirements between the same BD and evacuation pressure levels. The recovery can be increased by increasing the working capacity of the bed by going lower in evacuation pressure, implying a higher vacuum pump penalties. Further improvements to the monolithic process design are still possible by increasing the adsorbent density in the column (for example, by increasing the adsorbent layer thickness) and further increasing the interstitial velocity, until a point where the increased mass transfer resistance starts to significantly affect the performance. The monolithic CO_2 VPSA process design reported here has been focused primarily on retrofitting a small-scale SMR system. Further improvements in

overall efficiencies could be obtained considering a "greenfield" development where the H_2 PSA unit could be redesigned to take into account the reduction in overall flowrate and the increased H_2 concentration in the feed.

ASSOCIATED CONTENT

Table S1 listing the monolith characteristics.

Table S2 listing the fitted dual-site Langmuir isotherm parameters.

Figure S1 Adsorption isotherms for CH_4, CO, CO_2, H_2, N_2 and H_2O

Table S3 listing the pelleted-adsorbent and the packed bed characteristics

ACKNOWLEDGMENT

The authors would like to acknowledge the financial support from the Engineering and Physical Sciences Research Council, under the grant *Versatile Adsorption Processes for the Capture of Carbon Dioxide from Industrial Sources – FlexICCS* (EP/N024613/1).

ABBREVIATIONS

ADS: Adsorption

BD: Blowdown

CCS: Carbon Capture and Storage

D1: First de-pressurisation (equalisation)

D2: Second de-pressurisation (equalisation)

D3: Third de-pressurisation (equalisation)

D4: Fourth de-pressurisation (equalisation)

Evac: Evacuation

LDF: Linear Driving Force

LPP: Light product (H_2) pressurisation

Mt: Megatonnes

NG: Natural Gas

P1: First pressurisation (equalisation)

P2: Second pressurisation (equalisation)

P3: Third pressurisation (equalisation)

P4: Fourth pressurisation (equalisation)

PSA: Pressure Swing Adsorption

R: Rinse step

RP: Rinse pressurisation

SMR: Steam Methane Reforming

VPSA: Vacuum Pressure Swing Adsorption

SYMBOLS

A_{free}: Free cross-sectional area of a channel (m^2)

A_{ads}: Absorbent area of a channel (m^2)

$b_{j,0}^{l}$: Langmuir affinity parameter for component *j* on site l (1/bar)

$c_{ad,j}$: Concentration of component *j* in the adsorbent layer voids (mol/m^3)

c_j: Concentration of component *j* in bulk fluid phase (mol/m^3)

c_T: Total concentration in the bulk fluid phase (mol/m^3)

CT: Cycle time (s)

$\frac{dP}{dz}$: Pressure gradient along the axial length (Pa/m)

$D_{m,j}$: Molecular diffusivity of component *j* (m^2/s)

$D_{s,j}$: Diffusivity of component j in the adsorbent layer (assumed to be the same as molecular diffusivity) (m^2/s)

E_{BD}: Energy (electricity) consumed during BD step (kJ)

E_{Evac}: Energy (electricity) consumed during the evacuation step (kJ)

$\dot{E}_{CO_2}$: Energy (electricity) consumed per unit mol of CO_2 captured (kJ/mol CO_2)

$\dot{Ex}$: Specific exergy input (kJ/mol CO_2)

$\dot{Ex}_{MDEA}$: Specific exergy input to the MDEA process (kJ/mol CO_2)

$\dot{Ex}_{Shaft\ Work}$: Specific exergy input in the form of shaftwork (kJ/mol CO_2)

F_{BD}: Flow through the BD compressor (mol/s)

F_{max}: Maximum flow through the BD compressor (mol/s)

h: Free cross-sectional side length (individual channel) (m)

J_j: Diffusive flux of component j ($mol/m^2/s$)

$k_{LDF,j}$: LDF mass transfer co-efficient for component j (1/s)

L: Length of the monolith column (m)

m_{CO_2}: Moles of CO_2 obtained during evacuation step (mol)

$\dot{m}_{CO_2}$: Rate of CO_2 capture in MDEA literature sources (Mt/y)

m_{Feed}: Moles of feed processed per cycle (mol)

NC: Number of components

p_j: Partial pressure of component j (bar)

P_{BD}: Pressure at the end of the BD step (bar)

P_{Evac}: Pressure at the end of the evacuation step (bar)

P_{CO_2}: Purity of CO_2 product stream (%)

Q_{Reb}: Reboiler duty in MDEA process (MW)

R_{CO_2}: Overall recovery of CO_2 in CO_2 product stream (%)

q_j^*: Adsorbed phase concentration of component j at equilibrium (mol/m^3)

q_j: Adsorbed phase concentration of component j (mol/m^3)

$q_{j,s}^{l}$: Saturation capacity of component *j* for site *l* (mol/m^3)

$\overline{q_j}$: Average adsorbed phase concentration of component *j* (mol/m^3)

$\overline{Q_j}$: Average concentration of component *j* in the adsorbent layer (mol/m^3)

R: Universal gas constant (J/mol/K)

t: Time (s)

T: Temperature (K)

T_{Reb}: Reboiler temperature for MDEA process (K)

T_{amb}: Ambient Temperature (K)

v: Interstitial velocity in channels (m/s)

V_{bed}: Total volume of the adsorption beds (m^3)

w: Adsorbent layer thickness (individual channel) (m)

w_c: Corrected adsorbent layer thickness (individual channel) (m)

w_m: Metal layer half-thickness (individual channel) (m)

y_j: Mole fraction of component *j* in bulk fluid phase

z: Axial length (m)

Greek

$\Delta\widetilde{H}_j^l$: Heat of adsorption of component *j* on site *l* (J/mol)

ΔP: Pressure difference across the BD compressor (bar)

ε_{ad} : Porosity of the adsorbent layer

ε_{bulk}: Bulk porosity for channels

η: Dynamic viscosity of the gas (Pa s)

κ_{Feed}: Productivity of the VPSA unit in terms of feed processed (mol/m^3/s)

κ_{CO_2}: Productivity of the VPSA unit in terms of CO_2 produced (mol/m^3/s)

τ_{ad}: Tortuosity of the adsorbent layer pore network

χ: A constant (mol/s/bar^2)

REFERENCES

(1) IEAGHG. *Techno-Economic Evaluation of SMR Based Standalone (Merchant) Hydrogen Plant with CCS*; IEAGHG Technical Report 2017-02, February, 2017.

(2) Department for Business, Energy & Industrial Strategy. https://www.gov.uk/government/news/uk-becomes-first-major-economy-to-pass-net-zero-emissions-law (accessed September 19, 2019)

(3) Baade, W.F.; Farnand, S.; Hutchinson, R.; Welch, K. CO_2 capture from SMRs: A demonstration project. *Hydrocarbon Processing* **2012**, 91, 63-68.

(4) *Offset Project Plan for the Quest Carbon Capture and Storage Project*; Cap-Op Energy, December, 2015

(5) Tanaka, Y.; Sawada, Y.; Tanase, D.; Tanaka, J., Shiomi, S., Tetsuo, K. Tomakomai CCS Demonstration Project of Japan, CO_2 Injection in Process. *Energy Procedia* **2017**, *114*, 5836. DOI: 10.1016/j.egypro.2017.03.1721

(6) Air Liquide press release. https://www.airliquide.com/sites/airliquide.com/files/2015/11/05/world-premiere_air-liquide-inaugurates-its-co2-cold-capture-system-cryocap.pdf (accessed: 19-09-2019).

(7) *The Global Status of CCS : 2017*; Global CCS Institute, 2017.

(8) PRISM Hydrogen Generators (Air Products). http://www.airproducts.com/Microsites/phg-products.aspx (accessed: 19-09-2019).

(9) Schjølberg, I.; Hulteberg, C.; Yasuda, I.; Nelsson, C. Small scale reformers for on-site hydrogen supply. *Energy Procedia* **2012**, 29, 559-566. DOI: 10.1016/j.egypro.2012.09.065

(10) Rapid Cycle Pressure Swing Adsorption (RCPSA) brochure. http://www.xebecinc.com.cn/pdf/e_h2x_6200_brochure.pdf (accessed: 19-09-2019).

(11) Mohammadi, N. CO_2 capture from flue gas by a PSA process using a novel structured adsorbent. Ph.D. Thesis, The University of South Carolina, 2017

(12) Rezaei, F.; Mosca, A.; Webley, P.; Hedlund, J.; Xiao, P. Comparison of traditional and structured adsorbents for CO_2 separation by vacuum-swing adsorption. *Ind. Eng. Chem. Res.* **2010**, 49(10), 4832-4841. DOI: 10.1021/ie9016545

(13) Streb, A.; Hefti, M.; Gazzani, M.; Mazzotti, M. A novel adsorption process for co-production of hydrogen and CO_2 from a multicomponent stream. *Ind. Eng. Chem. Res.* **2019**, 58(37), 17489-17506. DOI: 10.1021/acs.iecr.9b02817.

(14) Harrison, D. P. Calcium enhanced hydrogen production with CO_2 capture. *Energy Procedia* **2009**, 1(1), 675–681. DOI: 10.1016/j.egypro.2009.01.089.

(15) Medrano, J. A.; Spallina, V.; Annaland, M.S.; Gallucci, F. Thermodynamic analysis of a membrane-assisted chemical looping reforming reactor concept for combined H_2 production and CO_2 capture. *International Journal of Hydrogen Energy* **2014**, 39, 4725–4738. DOI: 10.1016/j.ijhydene.2013.11.126.

(16) CORDIS EU Research Results. https://cordis.europa.eu/project/rcn/101420/reporting/en (accessed: 19-09-2019).

(17) Zhu, Q. Developments on CO_2-utilization technologies. *Clean Energy* **2019**, 3(2), 85–100. DOI: 10.1093/ce/zkz008.

(18) Sharma, I.; Friedrich, D.; Golden, T.; Brandani, S. Exploring the opportunities for carbon capture in modular, small-scale steam methane reforming: An energetic perspective. *International Journal of Hydrogen Energy* **2019**, 44, 14732–14743. DOI: 10.1016/j.ijhydene.2019.04.080.

(19) Maxwell, G. R. *Synthetic Nitrogen Products: A Practical Guide to the Products and Processes*; Kluwer Academic Publishers: New York, 2005; 57–90.

(20) VeloxoTherm™ Carbon Capture Technology. Emissions Reduction Alberta, https://www.eralberta.ca/projects/details/veloxotherm-carbon-capture-technology/ (last accessed November 10, 2019).

(21) Boot-Handford, M. E.; Abanades, J.C.; Anthony, E.J.; Blunt, M.J.; Brandani, S.; Mac Dowell, N.; Fernandez, J.R.; Ferrari, M.-C.; Gross, R.; Hallett, J.P.; Haszeldine, R.S.; Heptonstall, P.; Lyngfelt, A.; Makuch, Z.; Mangano, E.; Porter, R.T.J; Pourkashanian, M.; Rochelle, G.T.; Shah, N.; Yao, J.G.; Fennell, P.S. Carbon captore and storage update. *Energy & Environmenatal Science* **2014**, 7, 130–189. DOI: 10.1039/c3ee42350f.

(22) Shao, W.; Zhang, L.; Li, L.; Lee, R.L. Adsorption of CO_2 and N_2 on synthesized NaY zeolite at high temperatures. *Adsorption* **2009**, 15, 497–505. DOI: 10.1007/s10450-009-9200-y.

(23) Friedrich, D.; Mangano, E; Brandani, S. Automatic estimation of kinetic and isotherm parameters from ZLC experiments experiments. *Chemical Engineering Science* **2015**, 126, 616–624. DOI: 10.1016/j.ces.2014.12.062.

(24) Rastelli, H.; Chao, C. C.; Garg, D.R. Selective adsorption of CO_2 on Zeolites. U.S. Patent 4,775,396, Oct. 4, 1998.

(25) Harlick, P. J. E.; Tezel, F. H. Equilibrium analysis of cyclic adsorption processes: CO_2 working capacities with NaY. *Separation Science and Technology* **2005**, 40(13), 2569–2591. DOI: 10.1080/01496390500283233.

(26) Zhang, J.; Webley, P. A. In *Methodology For Screening Adsorbents For CO_2 Capture*, Proceedings of 2007 AIChE Annual Meeting, Salt Lake City, UT, November 4-9, 2007.

(27) Talu, O.; Zhang, S.; Hayhurst, D. T. Effect of Cations on Methane Adsorption by NaY, MgY, CaY, SrY, and BaY Zeolites. *J. Phys. Chem.* **1993**, 97, 12894–12898. DOI: 10.1021/j100151a043.

(28) Walton, K. S.; LeVan, M. D. *Separation of carbon monoxide and carbon dioxide for Mars ISRU*; Technical report for NASA, 2004.

(29) Raj, M. C.; Prasanth, K.P.; Dangi, G.P.; Bajaj, H.C. Hydrogen sorption in transition metal exchanged zeolite Y : volumetric measurements and simulation study. *Journal of Porous Materials* **2012**, 19(5), 657–666. DOI: 10.1007/s10934-011-9517-2.

(30) Pires, J.; Pinto, M. L.; Carvalho, A., Carvalho, M.B. Assessment of Hydrophobic-Hydrophilic Properties of Microporous Materials from Water Adsorption Isotherms. *Adsorption* **2003**, 9, 303–309. DOI: 10.1023/A:1026219813234.

(31) Hsu, K.-K.; Berg, J.J.; Xu, J.; Weist (Jr.), E.L. Adsorption Process. US Patent 8,709,136 B2, Apr. 29, 2014.

(32) Sircar, S.; Golden, T. C. Purification of Hydrogen by Pressure Swing Adsorption. *Separation Science and Technology* **2000**, 35(5), 667–687. DOI: 10.1081/SS-100100183.

(33) Friedrich, D.; Ferrari, M.; Brandani, S. Efficient Simulation and Acceleration of Convergence for a Dual Piston Pressure Swing Adsorption System. *Ind. Eng. Chem. Res.* **2013**, 52, 8897–8905. DOI: 10.1021/ie3036349.

(34) Kumar, R.; Fox, V.G.; Hartzog, D.G.; Larson, R.E.; Chen, Y.C.; Houghton, P.A.; Naheiri, T. A versatile process simulator for adsorptive separations. *Chemical Engineering Science* **1994**, 49(18), 3115–3125. DOI: 10.1016/0009-2509(94)E0085-5.

(35) Ahn, H.; Brandani, S. Dynamics of Carbon Dioxide Breakthrough in a Carbon Monolith Over a Wide Concentration Range. *Adsorption* **2005**, 11, 473–477. DOI: 10.1007/s10450-005-5970-z.

(36) Ahn, H.; Brandani, S. Analysis of breakthrough dynamics in rectangular channels of arbitrary aspect ratio. *AIChE Journal* **2005**, 51(7), 1980–1990. DOI: 10.1002/aic.10432.

(37) Luberti, M.; Friedrich, D.; Brandani, S. Design of a H_2 PSA for cogeneration of ultrapure hydrogen and power at an advanced integrated gasification combined cycle with pre-combustion capture. *Adsorption* **2014**, 20, 511–524. DOI: 10.1007/s10450-013-9598-0.

(38) Cornish, R. J. Flow in a pipe of rectangular cross-section. *Proceedings of the Royal Society A* **1928**, 120, 691–700.

(39) Farmahini, A. H.; Krishnamurthy, S.; Friedrich, D.; Brandani, S.; Sarkisov, L. From Crystal to Adsorption Column: Challenges in Multiscale Computational Screening of Materials for Adsorption Separation Processes. *Ind. Eng. Chem. Res.* **2018**, 57, 15491–15511. DOI: 10.1021/acs.iecr.8b03065.

(40) Quest Carbon Capture and Storage project: annual report (2018). Alberta's CCS Knowledge Sharing Program, https://open.alberta.ca/publications/quest-carbon-capture-and-storage-project-annual-report-2018 (last accessed November 10, 2019).

(41) Techno-Economic Evaluation of SMR based Standalone (Merchant) Hydrogen Plant with CCS; Technical Report No. 2017-02; IEAGHG, 2017.

(42) Basmadjian, D. Adsorption Equilibria of Hydrogen, Deuterium and their mixtures, Part I. *Can. J. Chem.* **1960**, 38, 141–148.

(43) Ruthven, D. M. *Principles of Adsorption and Adsorption Processes*; John Wiley & Sons: New York, 1984; 29–60.

Table of Contents (TOC)/Abstract Graphics: